In Vivo Imaging of ^{64}Cu-Labeled Polymer Nanoparticles Targeted to the Lung Endothelium

Raffaella Rossin[1], Silvia Muro[2,3], Michael J. Welch[1], Vladimir R. Muzykantov[2,3], and Daniel P. Schuster[†1,4]

[1]Mallinckrodt Institute of Radiology, Washington University School of Medicine, St. Louis, Missouri; [2]Institute for Environmental Medicine, University of Pennsylvania Medical School, Philadelphia, Pennsylvania; [3]Department of Pharmacology, University of Pennsylvania Medical School, Philadelphia, Pennsylvania; and [4]Department of Internal Medicine, Washington University School of Medicine, St. Louis, Missouri

Nanoparticles (NPs) targeting the intercellular adhesion molecule 1 (ICAM-1) hold promise as a mean of delivering therapeutics to the pulmonary endothelium in patients with acute and chronic respiratory diseases. As these new materials become available, strategies are needed to understand their behavior in vivo. We have evaluated the use of ^{64}Cu and PET to noninvasively image the lung uptake and distribution of NPs coated with an anti-ICAM antibody. **Methods:** Model fluorescent NPs were coated with a mixture of an anti-ICAM antibody (or nonspecific IgG) and ^{64}Cu-DOTA-IgG (where DOTA is 1,4,7,10-tetraazacyclododecane-1,4,7,10-tetraacetic acid). Biodistribution and small-animal PET and CT studies were performed in healthy mice and in mice pretreated with lipopolysaccharides (LPSs). Metabolism studies were also performed to evaluate the stability of ^{64}Cu-labeled NPs in lungs in vivo. **Results:** The lungs of mice administered anti-ICAM NPs labeled with ^{64}Cu were clearly imaged by small-animal PET 1, 4, and 24 h after administration. Both biodistribution and small-animal imaging showed a 3- to 4-fold higher uptake in the lungs of mice injected with ICAM-targeted NPs relative to that of the control group. Lung uptake was further enhanced by pretreating the mice with LPS, presumably because of ICAM-1 upregulation. However, an approximately 2-fold decrease in lung signal was observed in each experimental group over 24 h. Metabolism studies in lung tissues harvested from mice injected with ^{64}Cu-labeled anti-ICAM NPs showed considerable release of a small ^{64}Cu-radiometabolite from the NPs beginning as early as 1 h after injection. A decrease in lung fluorescence was also observed, most likely reflecting partial release of NPs from the lungs in vivo. **Conclusion:** The use of small-animal PET to track ^{64}Cu-labeled nanostructures in vivo shows potential as a strategy for the preclinical screening of new NP drug delivery agents targeting the lung endothelium and other tissues. Future design optimization to prolong the stability of the radiolabel in vivo will further improve this promising approach.

Key Words: ^{64}Cu; nanoparticles; ICAM-1; pulmonary endothelium; PET

J Nucl Med 2008; 49:103–111
DOI: 10.2967/jnumed.107.045302

Received Jul. 16, 2007; revision accepted Sep. 12, 2007.
For correspondence or reprints contact: Raffaella Rossin, PhD, Department of Biomolecular Engineering, Philips Research Laboratories, High Tech Campus 11, 5656 AE Eindhoven, The Netherlands.
E-mail: raffaella.rossin@philips.com
†Deceased.

A general problem in medicine is that therapeutic agents must often be administered in higher doses than otherwise desirable, thereby exposing the patient to unwanted toxicities to achieve the required concentration of drug in the diseased tissue. An important premise of current nanotechnology research is that nanoscale materials can be assembled, labeled, targeted, filled, and activated as needed to enhance drug delivery and reduce toxicity (*1–4*). Lung diseases—such as acute lung injury, cystic fibrosis, chronic obstructive lung disease, pulmonary hypertension, and others—could all benefit from such advances (*5*).

The lungs are unique among the various body organs in that drugs—including nanoparticles (NPs) carrying drugs—may be delivered to them via the airways or intravenously. Especially for lung diseases in which dysregulated endothelial function is an important component of pathogenesis, intravenous administration will often be the preferred route for NP delivery. Unfortunately, despite a variety of so-called "stealth" strategies, hepatic elimination of NPs is usually high and, as a consequence, lung accumulation of the materials will usually be low (*6,7*).

Immunotargeting of the pulmonary endothelium can be used to circumvent this problem by conjugating NPs with antibodies or other moieties directed to antigens, receptors, or other targets on the pulmonary endothelium (*3–5*). Recently, Muzykantov and colleagues have shown that lung delivery can be significantly enhanced by immunotargeting the pulmonary endothelium with monoclonal antibodies directed against intercellular adhesion molecule 1 (ICAM-1) (*8–16*). Although this immunoglobulin-like transmembrane endothelial adhesion molecule is constitutively expressed in the tissues of every organ, favorable pharmacokinetics (a result of the high-flow, high-capacity, low-resistance nature of the pulmonary vasculature) ensure relatively high lung extraction of materials coupled to anti-ICAM antibodies.

As nanomaterials are developed to carry drugs to the lungs, it will be important to be able to eventually monitor the success of drug delivery, release, activation, and effectiveness. In vivo imaging technologies should be ideally suited for these purposes. Among the available imaging

technologies, CT provides high spatial resolution but no method is readily available to label either the NP or its drug cargo for detection by CT. In contrast, nanomaterials can be appropriately labeled for MRI; however, the lungs are often poorly visualized with MRI because lung density is low compared with other soft tissues and because susceptibility artifacts resulting from the many air–tissue interfaces further reduce the MR signal (*17*). PET, instead, is a highly sensitive and quantitative imaging method that has been used repeatedly to image several lung functions, in both preclinical and clinical settings (*18–21*). Furthermore, the positron-emitting radionuclide ^{64}Cu has already been used to successfully image NP distribution in vivo, in both healthy animals (*22*) and disease models (*23,24*).

The purpose of the following proof-of-principle studies was to determine whether it would be possible to visualize and quantitate in real-time targeting of anti-ICAM nanocarriers to the lung endothelium of mice by using ^{64}Cu and PET.

MATERIALS AND METHODS

Antibodies and Reagents

Unless otherwise stated, all chemicals were purchased from Sigma-Aldrich and used without further purification. 1,4,7,10-Tetraazacyclododecane-1,4,7,10-tetraacetic acid mono(*N*-hydroxysuccinimide ester) (DOTA-NHS) was purchased from Macrocyclics. Monoclonal antibody recognizing the extracellular domain of murine ICAM-1 (YN1) was purified by affinity chromatography from the corresponding hybridoma cell line (American Type Culture Collection), and control IgG was obtained from Jackson ImmunoResearch Laboratories, Inc. Fluorescein isothiocyanate (FITC)-labeled polystyrene latex beads (100-nm diameter) were purchased from Polysciences. ^{64}Cu was prepared on the Washington University Medical School CS-15 Cyclotron (Cyclotron Corp.) by the ^{64}Ni(p,n)^{64}Cu nuclear reaction at a specific activity of 1.8–7.4 GBq/μg at the end of bombardment, as described (*25*). The buffers used for ^{64}Cu labeling were treated with Chelex-100 resin (Bio-Rad Laboratories) before use. Centricon tubes (YM-30: molecular weight cutoff, 30 kDa) were purchased from Millipore. Instant thin-layer chromatography (ITLC) plates (Pall ITLC-SG plates; VWR International) were developed in a 1:1 mixture of methanol and 10% (w/v) ammonium acetate and analyzed on a Bioscan 200 TLC scanner. Fast-protein liquid chromatography (FPLC) and radio-FPLC were performed using an ÄKTA FPLC system (GE Healthcare Biosciences) equipped with a Beckman 170 Radioisotope Detector (Beckman Instruments). A 100-μL analyte of the labeled NP was injected into a Superose 12 gel-filtration column (GE Healthcare Biosciences) and eluted with 20 mmol/L *N*-(2-hydroxyethyl)piperazine-*N*′-(2-ethanesulfonic acid) (HEPES) and 150 mmol/L NaCl (pH 7.3) at 0.8 mL/min. The UV wavelength was preset to 280 nm.

Synthesis of ^{64}Cu-Labeled Immunobeads

IgG conjugation to DOTA and ^{64}Cu radiolabeling were achieved by using standard procedures (*22*). IgG and DOTA-NHS (1:200 stoichiometric ratio) were mixed in 0.1 mmol/L Na_2HPO_4 (pH 7.5) at 4°C overnight. DOTA-IgG was separated from the excess reagent by extensive Centricon purification and was then recovered in phosphate buffer and stored at 4°C for later use. Radiolabeling was achieved by incubating DOTA-IgG (10 μg) and $^{64}CuCl_2$ (~11.1 MBq [300 μCi]) in 0.1 mmol/L ammonium citrate buffer (pH 5.5) at 37°C. After a 1-h incubation and challenge with diethylentriaminepentaacetic acid (DTPA), the radiolabeling yield was assessed by radio-TLC (^{64}Cu-DOTA-IgG, R_f = 0.0; ^{64}Cu-DTPA, R_f = 0.9). The mixture containing ^{64}Cu-DOTA-IgG (~1.1 MBq/μg) was used without further purification, as ^{64}Cu-DTPA was found not to interact with the polystyrene beads (data not shown). ^{64}Cu-Radiolabeled targeted and control NPs (^{64}Cu-(anti-ICAM)NPs and ^{64}Cu-(IgG)NPs, respectively) were obtained by coating the latex beads (NPs) with a 10:90 mixture of ^{64}Cu-DOTA-IgG/anti-ICAM-1 or ^{64}Cu-DOTA-IgG/IgG, respectively, for 1 h at room temperature (~75% coating efficiency). The coated beads were separated by centrifugation (4 min, 12,000 rpm), and the clear supernatant solution, containing unbound proteins and ^{64}Cu-DTPA, was removed. Then, the coated NPs were resuspended in 0.3% (w/v) bovine serum albumin in phosphate-buffered saline (PBS) and microsonicated at low power for 20 s (*26*). As shown previously by Muro et al. (*26*), this procedure produces a coating of ~250 IgG molecules per particle (i.e., ~7,000 IgG molecules/μm^2 particle surface), resulting in a particle ~180 nm in diameter (*11*). Furthermore, the antibodies were stably anchored to the NP surface and were not removed by additional washings.

In Vivo Studies

All animal studies were performed in compliance with guidelines set by the Washington University Animal Studies Committee. In general, male C57BL/6 mice (~20-g body weight) were anesthetized with 1%–2% vaporized isoflurane. Mice were then divided into 5 groups: groups 1 and 2 were used for a pilot biodistribution study. Groups 3–5 were used for a combined imaging/biodistribution study (Fig. 1). Groups 1 and 3 were injected with ^{64}Cu-(IgG)NPs (~1 × 10^{12} NPs coated with IgG/^{64}Cu-DOTA-IgG), whereas groups 2, 4, and 5 were injected with ^{64}Cu-(anti-ICAM)NPs (same number of NPs, in this case coated with ~45 μg

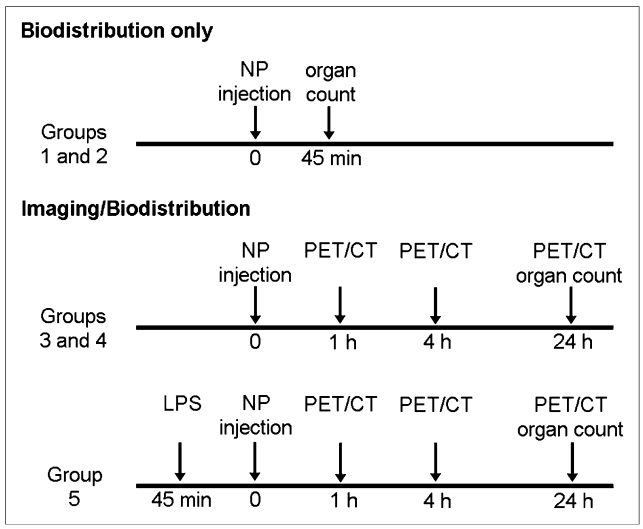

FIGURE 1. Time line of pretreatment, NP administration, and imaging/biodistribution time points. Groups 1 and 3 were administered ^{64}Cu-(IgG)NPs. Groups 2, 4, and 5 were administered ^{64}Cu-(anti-ICAM)NPs.

of anti-ICAM antibody and ^{64}Cu-DOTA-IgG). In addition, group 5 animals were treated intraperitoneally with lipopolysaccharide (LPS) from *Escherichia coli* 055:B5 (20 μg/g mouse body weight in 0.4–0.5 mL saline) to upregulate ICAM-1 expression (*13,27*) 45 min before the NPs were administered. In all cases, the radiolabeled material (~0.37 MBq for biodistribution and ~3.7 MBq for imaging/biodistribution studies) was injected in 110 μL 0.3% bovine serum albumin via the tail vein.

Biodistribution Studies

In a pilot study, organs from mice in groups 1 and 2 ($n = 4$ per group) were harvested 45 min after NP administration. On harvesting, tissues of interest were removed and blotted dry, and the radioactivity was measured in a well counter. The total activity in blood was calculated, assuming that the blood volume represented 7% of the mouse body weight. Diluted standard doses (1:100) were prepared and counted along with the samples. All data were corrected for ^{64}Cu decay and reported as percentage injected dose per gram tissue (%ID/g) and percentage injected dose per organ (%ID/organ) ± SD.

Imaging Studies

The mice in groups 3–5 were imaged 1, 4, and 24 h after NP administration. The imaging studies were performed using the microPET Focus 120 and 220 scanners (Siemens Medical Solutions, Inc.) and the MicroCAT II scanner (CTI-Imtek). Image coregistration was accomplished using a landmark registration technique (by using fiducial markers directly attached to the animal bed) and AMIRA image display software (Mercury Computing Systems). Data analysis of microPET images was performed on whole-lung region of interests (single slice) approximately 8 mm above the liver and diaphragm, drawn on the CT image (AMIRA). The data (corrected for radioactive decay of ^{64}Cu and normalized for injected activity) were calculated in terms of percentage injected dose per volume unit (%ID/mL) ± SD ($n = 4$ or 5). At the end of the imaging sessions, the lungs and other organs were harvested for biodistribution studies.

Metabolism Studies

Blank organ control experiments were performed by adding ^{64}Cu-(anti-ICAM)NPs, ^{64}Cu-DOTA-IgG (>98% radiochemical purity), or ^{64}Cu-citrate ex vivo to lung tissues harvested from untreated C56BL/6 mice immediately before workup. ^{64}Cu-(anti-ICAM)NPs were injected into C56BL/6 mice ($n = 3$) via the tail vein. At 1 and 24 h after injection, the mice were sacrificed, blood was aspirated, and the lungs were immediately excised, blotted dry, and placed on ice. Aliquots of tissue samples (~0.1 g) were homogenized in 0.1 mmol/L ammonium citrate (pH 5.5) using a Tissumizer tissue homogenizer (Tekmar) followed by a 30-s high-power tip-sonication using a Sonifier 185 cell disruptor (Branson). The insoluble proteins, cellular debris, and beads were separated by centrifugation (23,500*g*, 30 min, 4°C). One hundred microliters of each lysate were analyzed by FPLC. The radioactivity in pellets, lysates, and FPLC fractions (0.8 mL) was measured in a Beckman γ-8000 well counter. For all analyzed samples, >95% of the radioactivity was recovered from the size-exclusion column.

Fluorescence Studies

Aliquots of the lung tissues used for the metabolism studies (0.1 g) were homogenized in 200 μL PBS and microsonicated. The fluorescence (485 nm) of the homogenized samples was measured on a BioTek Synergy II (BioTek Instruments Inc.). Similar amounts of nontreated lung tissues added with a serially diluted bead suspension were homogenized and used to calculate a calibration curve.

Microscopy Studies

Lung samples obtained from mice injected with either (anti-ICAM)NPs or (IgG)NPs ($n = 2$) were harvested at 30 min or 24 h after injection and snap-frozen. Accumulation of green fluorescent NPs in the lungs was visualized by fluorescence microscopy from 10-μm-thick sections (3 slides per animal), on staining cell nuclei with blue 4,6-diamino-2-phenylindole (DAPI). The samples were analyzed by fluorescence microscopy using an Eclipse TE2000-U microscope, a 20× objective (Nikon), and an Orca-1 charge-coupled device camera (Hamamatsu).

Statistical Analysis

Group variation was described as the mean ± SD. Group comparisons were made using standard ANOVA methods. In some cases (e.g., figure legends), data were log-transformed to achieve normal data distributions. Post hoc testing of individual group differences was accomplished with the Holm–Sidak test. Groups with $P < 0.05$ were considered significantly different. Sigma-Stat software (version 3.1; Sysstat Software, Inc.) was used for all statistical calculations.

RESULTS

Biodistribution Studies

A pilot biodistribution study was first performed to determine whether immunotargeting ^{64}Cu-labeled NPs with anti-ICAM antibody resulted in measurable increases in lung radioactivity 45 min after NP injection. In fact, a 3.7 ± 1.1 ratio was found between the mean radioactivity in the lungs of group 2 and group 1 mice, consistent with enhanced uptake by the lung endothelium after administration of ICAM-targeted NPs. On the basis of these encouraging results, imaging studies in additional mice were performed 1, 4, and 24 h after NP administration in groups 3–5. On completion of the imaging studies (24 h after NP administration), organs were harvested once more for biodistribution measurements. The combined data of the 2 biodistribution studies are presented in Tables 1 and 2. The results of these experiments again showed increased lung uptake of immunotargeted NPs (group 4), with an additional increase in animals pretreated with LPS (group 5).

At both 1 and 24 h, little residual radioactivity was found in blood and heart, whereas a high amount of radioactivity was found in the organs of the mononuclear phagocyte system (MPS), such as liver and spleen. Liver uptake in the LPS-pretreated group at 24 h was the lowest among the 3 experimental groups, probably because of the higher NP accumulation in the lungs during the previous 24 h in this group. Also, a small amount of radioactivity was observed in the kidney, likely due to partial in vivo metabolism of the NPs' protein coat with urinary elimination of low-molecular-weight radioactive species. The biodistribution in whole

TABLE 1
Biodistribution Data of Selected Organs in C57BL/6 Mice at Time of Harvesting

	%ID/g				
	^{64}Cu-(IgG)NPs		^{64}Cu-(anti-ICAM)NPs		LPS + ^{64}Cu-(anti-ICAM)NPs
Organ	45 min	24 h	45 min	24 h	24 h
Blood	3.1 ± 0.3	1.6 ± 0.7	3.4 ± 0.4	2.2 ± 1.4	2.7 ± 0.7
Heart	0.8 ± 0.1	1.4 ± 0.7	1.3 ± 0.3*	1.9 ± 0.9	2.9 ± 1.0
Lung	29.6 ± 1.6	6.0 ± 4.6†	110.4 ± 33.3*	26.6 ± 29.3†	66.6 ± 35.7‡
Kidney	6.1 ± 0.6	7.4 ± 03.8	7.5 ± 1.2	9.7 ± 4.0	12.8 ± 1.2
Spleen	84.7 ± 18.2	72.7 ± 39.5	62.0 ± 14.4	82.4 ± 16.7	63.8 ± 18.2
Liver	48.23 ± 0.85	49.6 ± 7.7	32.4 ± 4.0*	42.3 ± 9.2	35.6 ± 4.1‡

*$P < 0.05$ compared with ^{64}Cu-(IgG)NP data at 45 min.
†$P < 0.05$ compared with data at 45 min (same tracer).
‡$P < 0.05$ compared with ^{64}Cu-(IgG)NP data at 24 h.
Data are presented as %ID/g tissue ± SD (n = 4 or 5).

organs at 24 h (Table 2) is similar to that observed on a "per gram" basis (Table 1). The principal effect of immunotargeting was an increase in NP uptake in the lungs and a decrease in the liver.

Imaging Studies

microPET images showed increased uptake of anti-ICAM–coated-NPs in the thoracic area as early as 1 h after NP administration (Figs. 2B and 2D). In fact, at this time point, the lungs of group 4 mice were clearly imaged by microPET, whereas the imaging signal in the lungs of group 3 mice was low. Furthermore, a presumed increased expression of ICAM on the endothelial surface after LPS administration before the imaging session (group 5) further increased the lung uptake of ^{64}Cu-(anti-ICAM)NPs at each time point (Fig. 3). At 1 h after injection, no detectable levels of radioactivity were observed in the heart of any of the imaged mice, confirming fast elimination of both ^{64}Cu-(anti-ICAM)NPs and ^{64}Cu-(IgG)NPs from the bloodstream, whereas a low amount of activity was observed in the bladder. In contrast, significant radioactivity accumulation was observed in the abdominal area due to NP uptake in MPS organs (liver and spleen; Fig. 2B).

Quantitative analysis of PET and CT images is shown in Figure 4. At 1 h after injection, the radioactivity in the lungs of group 3 mice was, on average, 3.8 and 2.4 times lower than that of group 5 and 4 mice, respectively. Furthermore, a steady decrease in lung radioactivity was observed over time. In fact, the radioactivity levels in both groups 4 and 5 decreased by a factor of ~2 over the 24-h period of observation (Fig. 4, top). A minor decrease was observed also in mice administered nonimmunotargeted beads (group 3). The changes in lung tissue radioactivity, as measured by imaging, were not due to differences in lung inflation as no significant changes in lung density were observed at any time point, as measured by CT (Fig. 4, bottom).

Metabolism Studies

To determine whether the decrease in lung tissue radioactivity over time was due to dissociation of the Cu label from the beads, the fate of the ^{64}Cu-(anti-ICAM)NPs in vivo was investigated in lung samples harvested from treated mice that were sacrificed at 1 and 24 h after injection (Table 3). The lung tissues were homogenized and centrifuged. Then, the percentage radioactivity recov-

TABLE 2
Biodistribution Data of Selected Organs in C57BL/6 Mice at 24 Hours After Injection

	%ID/organ		
Organ	^{64}Cu-(IgG)NPs	^{64}Cu-(anti-ICAM)NPs	LPS + ^{64}Cu-(anti-ICAM)NPs
Blood	0.5 ± 0.2	1.0 ± 0.7	0.7 ± 0.2
Heart	0.2 ± 0.1	0.2 ± 0.1	0.4 ± 0.1
Lung	0.9 ± 0.7	3.8 ± 4.0	10.5 ± 5.9*
Kidney	1.3 ± 0.7	1.6 ± 0.7	2.3 ± 0.2
Spleen	4.1 ± 1.8	4.7 ± 0.8	4.8 ± 1.3
Liver	59.8 ± 1.8	46.8 ± 7.1*	43.2 ± 3.0*

*$P < 0.05$ compared with ^{64}Cu-(IgG)NP data.
Data are presented as %ID/organ ± SD (n = 4 or 5).

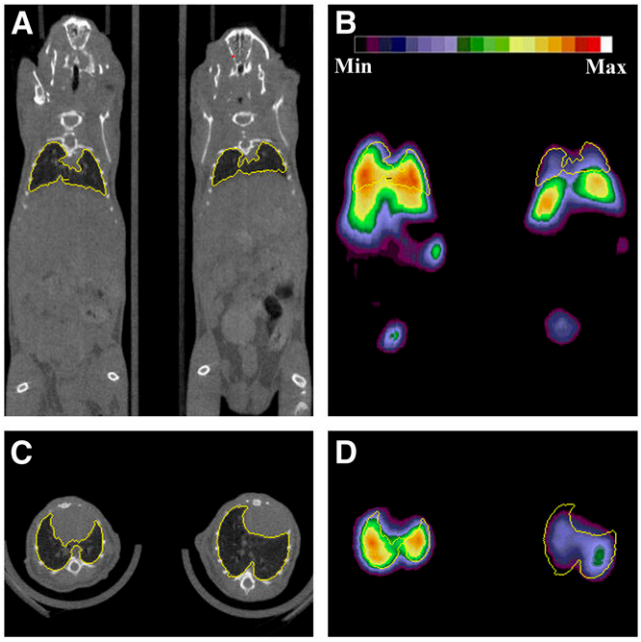

FIGURE 2. MicroCT (A, coronal slice; C, transverse slice) and microPET (B, coronal slice; D, transverse slice) images of 2 healthy C67BL/6 mice from group 3 (right) and group 4 (left) (~3.7 MBq per mouse, ~10^{12} NPs coated with 45 μg anti-ICAM/IgG per mouse). Yellow line indicates region of interest involving whole lungs. Min = minimum; Max = maximum.

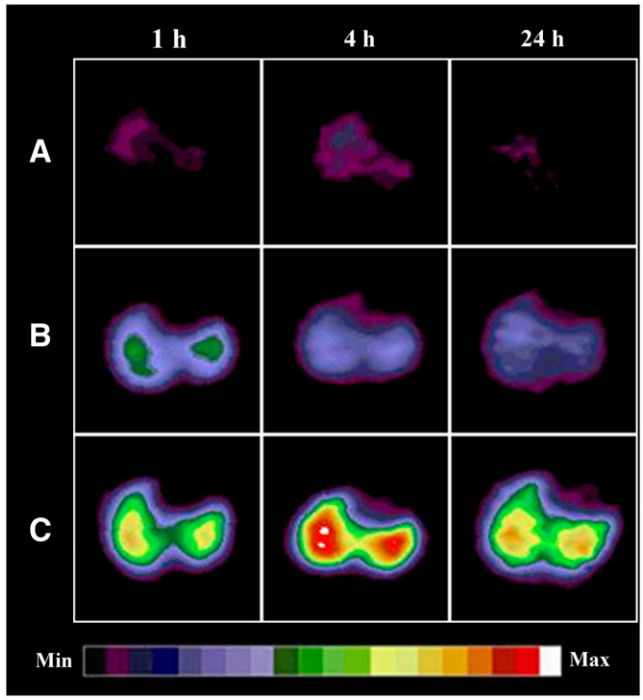

FIGURE 3. Representative decay-corrected transverse microPET images of mice from groups 3 (A), 4 (B), and 5 (C) at 1, 4, and 24 h after NP administration (~3.7 MBq per mouse, ~10^{12} NPs coated with 45 μg anti-ICAM/IgG per mouse). Min = minimum; Max = maximum.

ered in the pellet and supernatant solution was used to calculate the extraction efficiency (E = % activity in the supernatant/% activity in the pellet). Control organ blank experiments were performed to ensure that the species observed after NP intravenous injection were indeed the result of in vivo processes and not the consequence of homogenization or sonication. When ^{64}Cu-(anti-ICAM)NPs were added to the lungs of an untreated mouse ex vivo (control 1), >94% radioactivity was recovered in the insoluble residue (E = 0.06), and the small amount of lost radioactivity was due to partial dissociation of ^{64}Cu-DOTA-IgG from the particle, which was recovered in the soluble fraction as confirmed by radio-FPLC analysis (72% purity; Fig. 5A). On the contrary, when ^{64}Cu-DOTA-IgG was added to lung tissue ex vivo (control 2), >90% activity was recovered in solution as intact tracer (98% purity), whereas <10% of the initial ^{64}Cu was associated with insoluble proteins (E = 10.02). Finally, when treating lung tissue ex vivo with ^{64}Cu-citrate (control 3), the radioactivity distributed evenly between the insoluble and soluble fractions (E = 0.84).

When this procedure was performed on the lungs harvested 1 h after mice were administered ^{64}Cu-(anti-ICAM)NPs, 58% ± 3% of the total radioactivity was associated with the insoluble fraction of the tissue homogenate at 1 h after injection (E = 0.71 ± 0.08). Furthermore, only a minor fraction of the soluble metabolites containing ^{64}Cu eluted from the size-exclusion column with a retention time similar to that of ^{64}Cu-DOTA-IgG (24% ± 5% of total eluted activity; Fig. 5B), whereas 51% ± 11% of the activity was associated with a low-molecular-weight metabolite. These findings suggest metabolism of the NP-radiolabeled IgG protein coat in the lungs in vivo. At 24 h after injection, again, the radioactivity in the lung homogenate was evenly distributed between the soluble and the insoluble components (E = 0.72 ± 0.16), but almost no intact ^{64}Cu-DOTA-IgG was detected in the radio-FPLC chromatogram. These results, together with the decrease in lung radioactivity observed both in the biodistribution and in the imaging experiments, suggest complete degradation of the ^{64}Cu-labeled conjugate by this time point.

Fluorescence measurements on lung tissue homogenates (Fig. 6) showed a decrease in lung signal over time. Despite high autofluorescence and scattering in the analyzed suspensions, 3.8 ± 1.2 × 10^{10} fluorescent NPs per gram were detected in the lung tissues obtained from mice sacrificed 1 h after the administration of ^{64}Cu-(anti-ICAM)NPs. In contrast, the fluorescent signal in lungs 24 h after injection did not rise above the background, indicating the presence of <10^{10} fluorescent NPs per gram tissue (P = 0.02), as determined by comparison with a calibration curve obtained by adding known amounts of NPs to lung tissue ex vivo.

Fluorescence microscopy images of lung sections obtained after the intravenous injection of FITC-labeled NPs in additional mice are shown in Figure 7. Whereas the

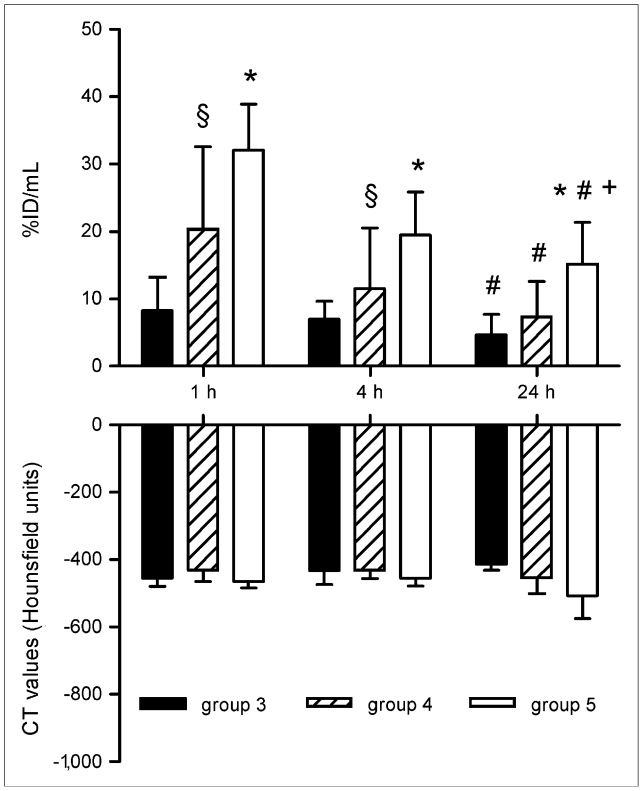

FIGURE 4. (Top) Comparative radioactivity uptake in lungs of mice of groups 3–5 obtained from quantitation of transverse microPET images (as in Fig. 3). Data are decay corrected and normalized for injected dose and are expressed as %ID/mL; error bars represent SD ($n = 4$ or 5). Statistical analysis: $^{*}P < 0.05$ compared with group 3; $^{+}P < 0.05$ compared with group 4; $^{\#}P < 0.05$ compared with 1 and 4 h; $^{\S}P < 0.05$ compared with 1 h. (Bottom) Lung density measurements, expressed as CT Hounsfield units, from analysis of CT scans, as in Figure 2. There were no statistically significant differences among any of mean values.

tissues from mice administered with control (IgG coated) NPs did not show any detectable fluorescence (left), sections obtained from mice administered (anti-ICAM)NPs showed the presence of green fluorescent NPs at both 30 min and 24 h after injection. Also, the ratiometric determination of FITC to DAPI fluorescence was consistent with an approximate 25% release of NPs from the lungs during the 24-h period.

DISCUSSION

ICAM-1 is an attractive target for immunotargeting drug carriers to the lung endothelium because of its high constitutive expression on endothelial cells (ECs), which can be further upregulated by pathologic factors, such as exposure to endotoxins, cytokines, oxidants, and so forth (*8,13,27*). In previous studies, immunoconjugates and fusion proteins targeting CAMs were able to specifically redirect antithrombotic and antioxidant enzymes to the lung endothelium (*8–10,15,16*). However, although these monomeric immunoconstructs exhibited avid binding to the target, poor internalization in ECs was observed both in vitro and in vivo (*10*). Conversely, multimeric nanoscale conjugates (<500 nm) obtained by coating beads with anti-ICAM antibodies were rapidly internalized in ECs via a unique endocytic process induced by ICAM clustering (*28*).

In healthy mice, administration of ^{125}I-labeled anti-ICAM NPs achieved lung uptake 1 order of magnitude higher than that of nontargeted NPs and 3 times higher than that of anti-ICAM alone shortly after administration (*11,29*). Therefore, we decided to explore the combined use of ICAM-1 targeting and PET to quantitatively evaluate the uptake and distribution of nanocarriers with potential use for drug delivery to the pulmonary endothelium. To accomplish this aim, we chose ^{64}Cu, a radionuclide used for PET of various disease states and radiotherapy (*30*). The approach for NP ^{64}Cu labeling was modified from that used by Muro et al. to label polystyrene NP with radioiodine (*11,28,29*).

A preliminary biodistribution experiment in healthy mice (Table 1) showed enhanced uptake of ^{64}Cu-(anti-ICAM)NPs by the lungs, presumably via the pulmonary endothelium. In fact, shortly after injection, the lung accumulation of radioactivity in group 2 mice was significantly higher than that in group 1 mice. Previous studies have shown that this increased uptake is not due to nonspecific uptake as a result of interactions with Fc receptors (as IgG-coated NPs also contain Fc receptors) or to mechanical entrapment of beads in the lung capillaries (*11,29*). Both targeted and control NPs were eliminated rapidly from the blood circulation. Furthermore, because of high uptake in the lungs, the amount of anti-ICAM NPs in MPS organs was significantly lower than that of nontargeted NPs, as previously reported for ^{125}I-labeled NPs (*11,29*).

TABLE 3
Extraction Efficiency (E) in Control Samples and Lung Samples 1 and 24 Hours After ^{64}Cu-(Anti-ICAM)NP Injection

Parameter	Control 1*	Control 2*	Control 3*	1 h	24 h
E†	0.06	10.02	0.84	0.71 ± 0.08	0.72 ± 0.16

*Control 1–3 = mouse lung added with ^{64}Cu-(anti-ICAM)NPs, ^{64}Cu-DOTA-IgG, or ^{64}Cu-citrate ex vivo, respectively.
†E = % radioactivity in supernatant/% radioactivity in pellet.
Data are presented as mean ± SD ($n = 3$).

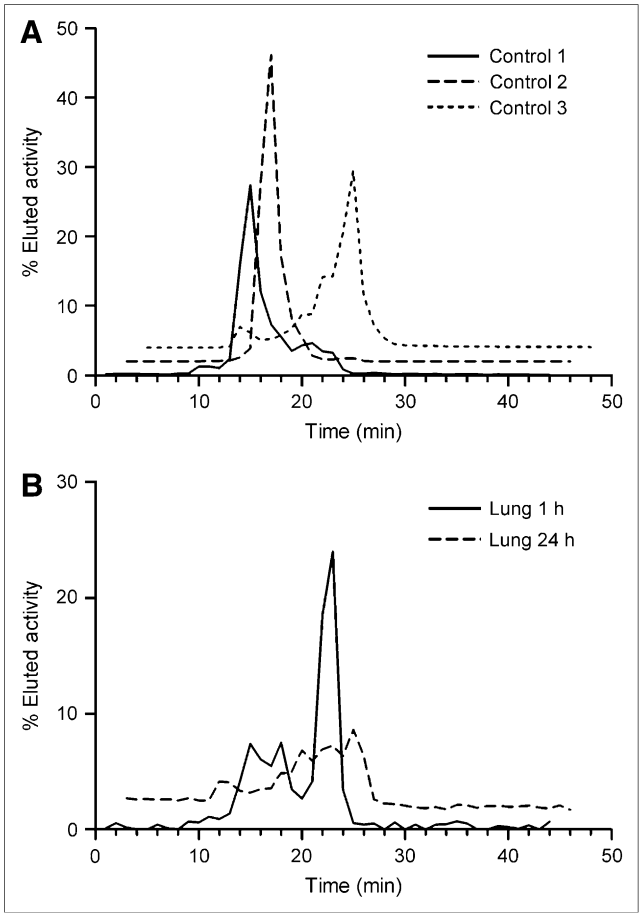

FIGURE 5. Metabolism studies: FPLC chromatograms of supernatant solutions obtained from homogenized blank lung tissues treated with ^{64}Cu-(anti-ICAM)NPs (control 1), ^{64}Cu-DOTA-IgG (control 2), or ^{64}Cu-citrate (control 3) ex vivo (A) and lung samples harvested from mice 1 and 24 h after intravenous administration of ^{64}Cu-(anti-ICAM)NPs (^{64}Cu-DOTA-IgG, retention time [R_t] = 15 min; ^{64}Cu-citrate, R_t = 22 min) (B).

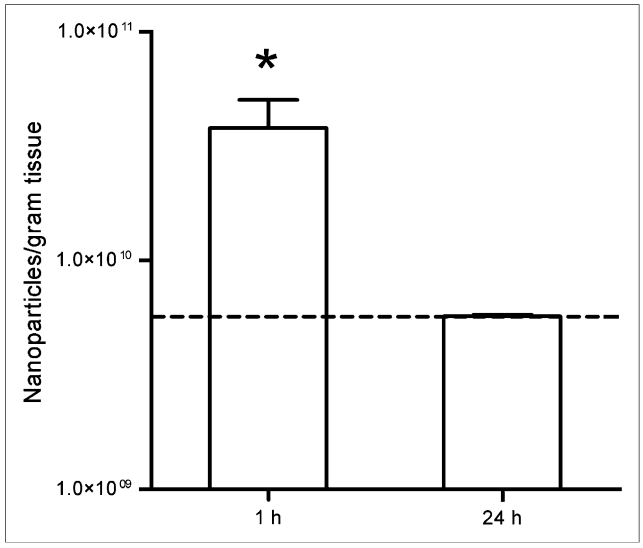

FIGURE 6. Fluorescence of homogenized lung samples harvested from C57BL/6 mice (n = 3) 1 and 24 h after administration of ^{64}Cu-(anti-ICAM)NPs (*P = 0.02). Dashed line indicates detection limit due to lung autofluorescence and tissue absorption.

microPET confirmed ICAM-1–targeted accumulation of ^{64}Cu-radiolabeled NPs in mouse lungs. In fact, the lungs of the animals in group 3 were clearly imaged at each time point (Fig. 3), whereas the liver was the only clearly visible organ in the group 1 mice (Fig. 2B). In addition, imaging contrast in lung tissue was further enhanced after pretreating the mice intraperitoneally with bacterial LPS (group 5; Fig. 3C). This effect is unlikely to have been caused by the influx of inflammatory cells. In fact, although LPS causes leukocyte sequestration in the lungs, inflammatory cells do not express ICAM-1 at high levels compared with endothelium, especially after stimulation with inflammatory mediators (*31,32*).

Both the biodistribution data (Table 1) and the quantitative analysis of microPET images (Fig. 4, top) revealed a slow decrease of radioactivity in lung tissue over the 24-h observation period in all experimental groups. In vivo transchelation of radiocopper from tetraazamacrocyclic chelates such as DOTA and triethylenetetramine has been observed previously in rodents (*33,34*) and in humans (*35–37*). The proposed mechanism for in vivo copper transchelation involves the reduction of Cu(II) to Cu(I) followed by release of the radiometal from the chelator. As a result of the change in oxidation state, the release of copper from the chelate is followed by the free radiometal binding to copper-avid proteins, such as superoxide dismutase, metallothioneins, ceruloplasmin, and others (*34,38*). In our studies, addition of ^{64}Cu-(anti-ICAM)NPs to mouse lung ex vivo did not produce significant degradation during the experimental procedure: Most of the radioactivity was recovered in the insoluble fraction of the homogenate (which can reasonably be assumed to be intact beads), whereas the small amount of radioactivity in solution exhibited the elution pattern of ^{64}Cu-DOTA-IgG. On the other hand, when processing mouse lungs 1 h after intravenous administration of ^{64}Cu-(anti-ICAM)NPs, approximately half of the radioactivity

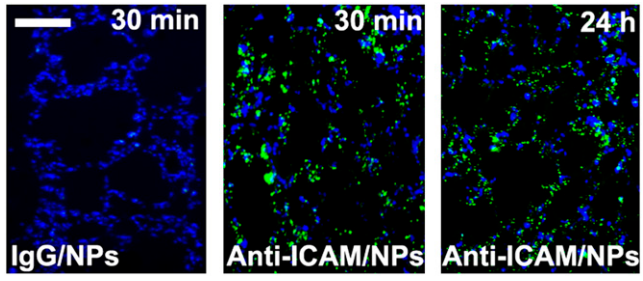

FIGURE 7. Representative fluorescence microscopy images (from n = 2 mice/experimental condition and 3 images per mouse) of lung sections from C57BL/6 mice injected intravenously with either FITC-labeled control (IgG)NPs or (anti-ICAM)NPs. Lungs were harvested 30 min or 24 h after injection. Cell nuclei were stained with blue DAPI. Scale bar = 100 μm.

was detected in solution, and the elution profile showed the presence of intact IgG (~25% of the total eluted activity), of a small-molecular-weight ^{64}Cu-metabolite (<5 kDa, ~50%), and of radiometabolites with intermediate molecular weight. Although the characterization of the metabolites and the implication of a mechanism for in vivo degradation are beyond the scope of this study, the data presented here clearly indicate dissociation of the radiolabel from the NPs in the lung in vivo. Therefore, the loss of lung radioactivity observed over time in our microPET and biodistribution experiments is at least partially—and perhaps, primarily—a consequence of radiometabolite release. In addition, the in vivo degradation of the immunoconjugates is possibly due to detachment of the ^{64}Cu-DOTA chelate used to tag the NPs or to loss of the radiometal while the nanosystems migrate intracellularly.

Despite clear metabolism of the radiolabeled protein coat, we also found evidence for at least partial release of NPs from the lungs over the 24-h period of observation (Figs. 6 and 7). Thus, in these studies at least, both the metabolism of the radiolabel and the loss of NPs themselves from the lungs contribute to the decrease in lung radioacitivity observed in both biodistribution and PET studies (Fig. 4; Table 1). In the future, better retention of the ^{64}Cu radiolabel on NPs in vivo can probably be achieved by using chelators with improved stability, such as the cross-bridged tetraazamacrocyclic and hexa-aza cage derivatives (*34,39*). Furthermore, the use of shell-core polymeric nanostructures bearing orthogonal functional groups can provide a means of covalently attaching targeting ligands on the surface of the nanocarrier, where they can easily access the target in vivo, while shielding the imaging probes and therapeutic cargo from in vivo metabolism and inactivation (*1,3,4,40,41*). These strategies should result in an improved ability to assess the pharmacokinetics and efficacy of nanomedicine for respiratory diseases by PET.

CONCLUSION

Nanomedicine brings together material and medical scientists for the development of more efficient diagnostic and therapeutic tools for cancer, lung, and cardiovascular diseases. In this study we investigated the possible use of PET to quantify the uptake of ICAM-1–targeted ^{64}Cu-labeled NPs by the pulmonary endothelium. Although both in vivo metabolism of ^{64}Cu-DOTA-conjugates and release of prototype nanocarriers from ECs led to a signal decrease with time, the lungs of mice injected with radiolabeled anti-ICAM NPs were clearly imaged by microPET up to 24 h after injection. Furthermore, increased contrast in the lungs was achieved when upregulating ICAM-1 with LPS administration. Therefore, this imaging approach holds promise for the validation of new drug delivery agents for respiratory diseases.

ACKNOWLEDGMENTS

We thank Dr. Zhaohui Zhou for assistance in bead preparation; Nicole Fettig, Margaret Morris, Dawn Werner, Amanda Roth, Lori Strong, Ann Stroncek, and James Kozlowsky for assistance in the biodistribution and imaging studies; John Leferovich for technical help with lung sections; Matt Bernstein for fluorescence measurements; and Tom Voller and Dr. Jason S. Lewis for ^{64}Cu production. This material is based on work supported by the National Institutes of Health as a Program of Excellence in Nanotechnology (grant HL080729) and, in part, by National Institutes of Health grants P30 DK47757, NHLBI RO1 HL71175, HL078785, and HL73940. The production of ^{64}Cu is supported by grant CA86307 from the National Cancer Institute.

REFERENCES

1. Brigger I, Dubernet C, Couvreur P. Nanoparticles in cancer therapy and diagnosis. *Adv Drug Deliv Rev.* 2002;54:631–651.
2. Brannon-Peppas L, Blanchette JO. Nanoparticle and targeted systems for cancer therapy. *Adv Drug Deliv Rev.* 2004;56:1649–1659.
3. Ding B-S, Dziubla T, Shuvaev VV, Muro S, Muzykantov VR. Advanced drug delivery systems that target the vascular endothelium. *Mol Interv.* 2006;6:98–112.
4. Torchilin VP. Multifunctional nanocarriers. *Adv Drug Deliv Rev.* 2006;58:1532–1555.
5. Pison U, Welte T, Giersig M, Groneberg DA. Nanomedicine for respiratory diseases. *Eur J Pharmacol.* 2006;533:341–350.
6. Moghimi SM, Hunter AC, Murray JC. Long-Circulating and Target-Specific Nanoparticles: Theory to Practice. *Pharmacol Rev.* 2001;53:283–318.
7. Owens DE III, Peppas NA. Opsonization, biodistribution, and pharmacokinetics of polymeric nanoparticles. *Int J Pharm.* 2006;307:93–102.
8. Atochina EN, Balyasnikova IV, Danilov SM, Granger DN, Fisher AB, Muzykantov VR. Immunotargeting of catalase to ACE or ICAM-1 protects perfused rat lungs against oxidative stress. *Am J Physiol Lung Cell Mol Physiol.* 1998; 275(4):L806–L817.
9. Ding B-S, Gottstein C, Grunow A, et al. Endothelial targeting of a recombinant construct fusing a PECAM-1 single-chain variable antibody fragment (scFv) with prourokinase facilitates prophylactic thrombolysis in the pulmonary vasculature. *Blood.* 2005;106:4191–4198.
10. Murciano J-C, Muro S, Koniaris L, et al. ICAM-directed vascular immunotargeting of antithrombotic agents to the endothelial luminal surface. *Blood.* 2003; 101:3977–3984.
11. Muro S, Dziubla T, Qiu W, et al. Endothelial targeting of high-affinity multivalent polymer nanocarriers directed to intercellular adhesion molecule 1. *J Pharmacol Exp Ther.* 2006;317:1161–1169.
12. Muro S, Mateescu M, Gajewski C, Robinson M, Muzykantov VR, Koval M. Control of intracellular trafficking of ICAM-1-targeted nanocarriers by endothelial Na^+/H^+ exchanger proteins. *Am J Physiol Lung Cell Mol Physiol.* 2006; 290:L809–L817.
13. Muro S, Muzykantov VR. Targeting of antioxidant and anti-thrombotic drugs to endothelial cell adhesion molecules. *Curr Pharm Des.* 2005;11:2383–2401.
14. Muro S, Schuchman EH, Muzykantov VR. Lysosomal enzyme delivery by ICAM-1-targeted nanocarriers bypassing glycosylation- and clathrin-dependent endocytosis. *Mol Ther.* 2006;13:135–141.
15. Muzykantov VR. Targeting of superoxide dismutase and catalase to vascular endothelium. *J Control Release.* 2001;71:1–21
16. Shuvaev VV, Dziubla T, Wiewrodt R, Muzykantov VR. Streptavidin-biotin crosslinking of therapeutic enzymes with carrier antibodies. In: Niemeyer CM, ed. *Methods in Molecular Biology.* Vol 283. Totowa, NJ: Humana Press; 2004: 3–9.
17. Garbow JR, Orellana CB, Neil JJ. Magnetic resonance imaging. In: Schuster DP, Blackwell TS, eds. *Molecular Imaging of the Lungs*. Vol 203. Boca Raton, FL: Taylor & Francis; 2005:113–133.
18. Bruzzi JF, Munden RF. PET/CT imaging of lung cancer. *J Thorac Imaging.* 2006; 21:123–136.

19. Bunyaviroch T, Coleman RE. PET evaluation of lung cancer. *J Nucl Med.* 2006; 47:451–469.
20. Chen DL, Schuster DP. Imaging pulmonary inflammation with positron emission tomography: a biomarker for drug development. *Mol Pharm.* 2006;3: 488–495.
21. Harris RS, Schuster DP. Visualizing lung function with positron emission tomography. *J Appl Physiol.* 2007;102:448–458.
22. Sun X, Rossin R, Turner JL, et al. An assessment of the effects of shell cross-linked nanoparticle size, core composition, and surface PEGylation on in vivo biodistribution. *Biomacromolecules.* 2005;6:2541–2554.
23. Rossin R, Pan D, Qi K, et al. ^{64}Cu-Labeled folate-conjugated shell cross-linked nanoparticles for tumor imaging and radiotherapy: synthesis, radiolabeling, and biologic evaluation. *J Nucl Med.* 2005;46:1210–1218.
24. Yuan J, You Y, Lu X, Muzik O, Oupicky D, Peng F. Synthesis of nano-sized poly(APMA)-DOTA-^{64}Cu conjugates for interventional radionuclide therapy of prostate cancer: assessment of intra-tumoral retention by microPET imaging. *Mol Imaging.* 2007;6:10–17.
25. McCarthy DW, Shefer RE, Klinkowstein RE, et al. Efficient production of high specific activity ^{64}Cu using a biomedical cyclotron. *Nucl Med Biol.* 1997;24: 35–43.
26. Muro S, Cui X, Gajewski C, Murciano J-C, Muzykantov VR, Koval M. Slow intracellular trafficking of catalase nanoparticles targeted to ICAM-1 protects endothelial cells from oxidative stress. *Am J Physiol Cell Physiol.* 2003;285: C1339–C1347.
27. Rothlein R, Jaeger JR. Treatment of inflammatory diseases with a monoclonal antibody to intercellular adhesion molecule 1. *Ciba Found Symp.* 1995;189: 200–208.
28. Muro S, Wiewrodt R, Thomas A, et al. A novel endocytic pathway induced by clustering endothelial ICAM-1 or PECAM-1. *J Cell Sci.* 2003;116:1599–1609.
29. Muro S, Gajewski C, Koval M, Muzykantov VR. ICAM-1 recycling in endothelial cells: a novel pathway for sustained intracellular delivery and prolonged effects of drugs. *Blood.* 2005;105:650–658.
30. Sun X, Anderson CJ. Production and applications of copper-64 radiopharmaceuticals. *Methods Enzymol.* 2004;386:237–261.
31. Dustin ML, Rothlein R, Bhan AK, et al. Induction by IL 1 and interferon-γ: tissue distribution, biochemistry, and function of a natural adherence molecule (ICAM-1). *J Immunol.* 1986;137:245–254.
32. Muro S. Intercellular adhesion molecule-1 and vascular cell adhesion molecule-1. In: Aird WC, ed. *Endothelial Biomedicine*. New York, NY: Cambridge University Press; 2007:1058–1079.
33. Bass LA, Wang M, Welch MJ, Anderson CJ. In vivo transchelation of copper-64 from TETA-octreotide to superoxide dismutase in rat liver. *Bioconjug Chem.* 2000; 11:527–532.
34. Boswell CA, Sun X, Niu W, et al. Comparative in vivo stability of copper-64-labeled cross-bridged and conventional tetraazamacrocyclic complexes. *J Med Chem.* 2004;47:1465–1474.
35. Anderson CJ, Dehdashti F, Cutler PD, et al. ^{64}Cu-TETA-octreotide as a PET imaging agent for patients with neuroendocrine tumors. *J Nucl Med.* 2001;42: 213–221.
36. DeNardo GL, DeNardo SJ, Kukis D, et al. Maximum tolerated dose of ^{67}Cu-2IT-BAT-LYM-1 for fractionated radioimmunotherapy of non-Hodgkin's lymphoma: a pilot study. *Anticancer Res.* 1998;18 (4B):2779–2788.
37. Mirick GR, O'Donnell RT, DeNardo SJ, Shen S, Meares CF, DeNardo GL. Transfer of copper from a chelated ^{67}Cu-antibody conjugate to ceruloplasmin in lymphoma patients. *Nucl Med Biol.* 1999;26:841–845.
38. Woodin KS, Heroux KJ, Boswell CA, et al. Kinetic inertness and electrochemical behavior of copper(II) tetraazamacrocyclic complexes: possible implications for in vivo stability. *Eur J Inorg Chem.* 2005;23:4829–4833.
39. Wadas TJ, Wong EH, Weisman GR, Anderson CJ. Copper chelation chemistry and its role in copper radiopharmaceuticals. *Curr Pharm Des.* 2007;13:3–16.
40. Wooley KL. Shell cross-linked polymer assemblies: nanoscale constructs inspired from biological systems. *J Polym Sci [A].* 2000;38:1397–1407.
41. Yang Y-Y, Wang Y, Powell R, Chan P. Polymeric core-shell nanoparticles for therapeutics. *Clin Exp Pharmacol Physiol.* 2006;33:557–562.

JNM The Journal of NUCLEAR MEDICINE

In Vivo Imaging of ^{64}Cu-Labeled Polymer Nanoparticles Targeted to the Lung Endothelium

Raffaella Rossin, Silvia Muro, Michael J. Welch, Vladimir R. Muzykantov and Daniel P. Schuster

J Nucl Med. 2008;49:103-111.
Published online: December 12, 2007.
Doi: 10.2967/jnumed.107.045302

The Journal of Nuclear Medicine is published monthly.
SNMMI | Society of Nuclear Medicine and Molecular Imaging
1850 Samuel Morse Drive, Reston, VA 20190.
(Print ISSN: 0161-5505, Online ISSN: 2159-662X)

SNMMI SOCIETY OF NUCLEAR MEDICINE AND MOLECULAR IMAGING